minerals

MDPI

Article

The Effect of Ionic Strength and Sr_{aq} upon the Uptake of Ra during the Recrystallization of Barite

Felix Brandt *, Martina Klinkenberg, Jenna Poonoosamy, Juliane Weber and Dirk Bosbach

Institute of Energy and Climate Research (IEK-6)—Nuclear Waste Management and Reactor Safety, Forschungszentrum Jülich GmbH, 52425 Jülich, Germany; m.klinkenberg@fz-juelich.de (M.K.); j.poonoosamy@fz-juelich.de (J.P.); weberj@ornl.gov (J.W.); d.bosbach@fz-juelich.de (D.B.)

* Correspondence: f.brandt@fz-juelich.de; Tel.: +49-2461-61-4205

Received: 21 September 2018; Accepted: 29 October 2018; Published: 2 November 2018

Abstract: Recrystallization and solid-solution formation with barite is considered as relevant retention mechanism for ^{226}Ra in long-term scenarios of nuclear waste management. Here, we studied the effect of ionic strength and the presence of Sr in solution upon the Ra-uptake kinetics and final Ra concentrations in solution by recrystallizing barite in solution with varying Sr and NaCl concentration and temperature for up to 1000 days. Final Ra-concentrations were interpreted based on thermodynamic modelling. Our results indicate a slight decrease of the retention potential of barite for Ra but little effect on the uptake kinetics due to the increase of ionic strength from. 0.1 mol/kg to 1.0 mol/kg of NaCl. The final concentrations at solid/liquid ratio of 0.5 g/kg are well described based on available thermodynamic models whereas at 5 g/kg additional Ra uptake probably due to kinetic effects was observed. On the contrary, the presence of Sr in solution can have a significant inhibiting kinetic effect on the uptake kinetics and lower the final Ra-uptake. In some cases, with low solid/liquid ratio or at ambient conditions, Sr completely inhibits barite recrystallization. In all other cases, Ra, Ba and Sr were taken up as thermodynamically predicted at the end of the experiments.

Keywords: radium uptake; recrystallization; (Sr,Ba,Ra)SO_4 solid solution; barite; celestine; ionic strength; nuclear waste management; ternary solid solutions

1. Introduction

Dissolution-reprecipitation reactions have been identified to play an important role not only during weathering reactions but also as key mechanism controlling mineral-mineral replacement reactions [1–3]. Within the last decade, replacement reactions at ambient and hydrothermal conditions have found increasing attention as examples for this dissolution-reprecipitation mechanism, starting from salt systems for example, KCl-KBr to carbonates [4,5], sulphates [6,7] to complex silicates [2,3].

A special case of such replacement reactions is the uptake of contaminants from aqueous solution during recrystallization and solid solution formation [6,8–12]. Here, the interaction of primary minerals with water and dissolved contaminants leads to a re-equilibration and the formation of a new solid solution. One of the most intensively studied systems is the group of sulphates isomorphic to barite, including the solid solutions between two or three of the end members of the $BaSO_4$- $SrSO_4$- $RaSO_4$- $PbSO_4$-system in contact with an aqueous solution. In contrast to co-precipitation which is a fast and well-studied process, full re-equilibration of sulphate powders can take from 3 up to several 1000 years [6,7,9,13,14].

Among the sulphates, the $RaSO_4$-$BaSO_4$-H_2O solid solution-aqueous solution system has received some attention because ^{226}Ra is considered to be relevant not only as important contributor to naturally occurring radioactive materials (NORM) occurring for example, at mining sites [15,16] but also as a

critical radionuclide with respect to the long-term safety of deep geological nuclear waste disposal. Therefore, the fate of ^{226}Ra in long-term scenarios has found special attention by safety case studies for example, for the high level nuclear waste repositories in Sweden or Switzerland [17,18]. In support of these safety case studies, experimental and theoretical studies were performed to fill the knowledge gaps of the thermodynamic data (e.g., [19–21]) or to experimentally verify the feasibility of the ^{226}Ra uptake into sulphate solid solutions by recrystallization and replacement reactions, reflecting the situation to be expected in a deep geological nuclear waste repository.

All of the recent recrystallization studies were carried out at close-to-equilibrium conditions. Recent experimental studies at low ionic strength confirmed the uptake of Ra into the binary $(Ba,Ra)SO_4$ solid solution as well as into the $(Sr,Ba,Ra)SO_4$ solid solution [11,12,20,22]. The studies by Klinkenberg et al. (2014) [10], Weber et al. (2016, 2017) [11,12] indicate the structural uptake of Ra into barite via a dissolution re-precipitation mechanism, based on microscopic evidence. A special role was attributed to the internal structure of barite which typically contains fluid inclusions. These fluid inclusions were present in the Sachtleben barite used in the studies by Klinkenberg et al. (2014) [10] and Weber et al. (2016, 2017) [11,12] and provided a pathway for radium to enter the crystal volume of barite. All these experiments started from a solid, which was put into contact with Ra, for example, $BaSO_4$ or the Sr-rich $(Sr,Ba)SO_4$ solid solution. The effect of ions in solution was so far only investigated during co-precipitation by Rosenberg et al., 2011 [13] with respect to ionic strength and regarding Sr in solution by Jucker and Treadwell, 1954 [23], Ceccarello et al., 2004 [24] and Ling et al., 2018 [25]. Background electrolytes can have a significant effect, not only on the solution thermodynamics but also on kinetic barriers for nucleation [8], barite growth rates [26–29] and barite crystal morphology [30]. In contrast, Sr in solution was observed to specifically interact with barite and Ra, inhibiting the co-precipitation with increasing Sr content in solution [24]. This indicates a competition of Sr in solution with Ra during the co-precipitation carried out by Ceccarello et al., 2014 [24]. On the other side, thermodynamic considerations based on atomistic calculations presented in Vinograd et al., 2018b [21] indicate that the optimum of Ra uptake can be expected in a Ba-rich $(Ba,Sr)SO_4$ with a ratio of Sr:Ba of about 1:10.

In contrast to previous studies which focused on Sr in the recrystallizing solid or on co-precipitation experiments, we laid the focus on the possible competition of Sr with Ra in solution during the recrystallization of barite. In earlier recrystallization studies by Klinkenberg et al. (2018) [10] and Vinograd et al. (2018) [21], $SrSO_4$ was present in the solid. In the first step of the equilibration process, these lead to the release of equivalent amounts of Sr and sulphate into the aqueous solution. Therefore, a combined effect of additional Sr and sulphate upon the uptake of Ra was studied which in some cases lead to intermediate phases of low solubility and a very dynamic recrystallization process regime. Here, we focus on the ions in solution, especially on Sr_{aq} and its effect on the structural uptake of Ra into pre-existing $BaSO_4$. In addition, the effect of ionic strength was monitored which allows for a separation of ionic strength effects from specific effects of additional Sr_{aq}. We used the same Sachtleben barite to make our results comparable with the earlier studies and assumed that the same dissolution re-precipitation mechanism would lead to a Ra-uptake during recrystallization. In order to test thermodynamic predictions regarding the equilibrium concentrations of Ba, Sr and ^{226}Ra, macroscopic batch experiments were not only performed at ambient temperature but also at elevated temperatures. Furthermore, the solid/liquid ratio was varied to investigate how the relationship between solution, solutes and available surface affects the Ra uptake.

2. Materials and Methods

The general batch experiment setup, including the barite powder and sampling procedure was adapted from earlier recrystallization studies (e.g., [7,10]) to enable a direct comparison of the new data. Batch recrystallization experiments were performed with barite at 90 °C, 80 °C and ambient conditions (23 ± 2 °C) using 20 mL of solution for each experiment. A commercially available high purity barite (Sachtleben® XR-HR 10 (Duisburg, Germany), Figure 1), which has been used as a reference in many

earlier studies (e.g., [6,22,31]), was adjusted to grain size dimensions higher than 10 µm (mean grain size: 15 µm) by a sedimentation technique and pre-equilibrated for four weeks at room temperature in 0.2 or 2.0 mol/kg NaCl solution, respectively, before the experiments to avoid high energy surface sites and ultrafine particles which may have an impact on the Ra uptake kinetics. This was the same procedure as in all our earlier studies to allow for comparison of the data. Detailed studies of the same batch of barite as used here showed that there were no other minerals or relevant contamination present. Klinkenberg et al. (2014) [10] determined a BET-surface area of 0.17 m^2/g for this barite powder. The 25 mL glass vessels used during the experiments were tested for wall adsorption of Ra and no measurable adsorption was detected.

The experiments were carried out with solid/liquid ratios of 5 g/kg and 0.5 g/kg, that is, 0.1 and 0.01 g of barite in 20 g of solution. All recrystallization experiments were started from a concentration of 5.0×10^{-6} mol/kg $RaBr_2$. High purity NaCl and $SrCl_2$ salts (Merck) were used to adjust the respective concentrations in solution. Samples of the aqueous solution were taken and analysed for ^{226}Ra by γ-spectroscopy and by inductively-coupled plasma mass-spectrometry (ICP-MS) for Sr or Ba, respectively. At regular time intervals 500 µL aliquots of the aqueous solution were taken and directly filtered after a settling time of 1 h through Advantec ultrafilters (MWCO = 10,000 Da). These filters were approved by earlier studies to exclude possible colloids or fine particles due to the close to equilibrium conditions of the experiments. The filters were tested and adsorption of Ra at the given filtered solution amount could also be excluded. The settling time of 1h was required for handling of the hot radioactive solutions (80, 90 °C). According to pre-tests the settling time is much shorter than the time required for barite and ^{226}Ra to re-equilibrate to the lower temperature. A N_2 cooled high purity (HP) Ge-detector was used for the quantification of the aqueous ^{226}Ra concentration (Ra_{aq}) via γ-spectrometry. The intensity of the Ra peak at 186 keV was determined and converted to a concentration unit (mol/kg). An independent, external standard was used for the calibration of the system. The aqueous Sr and Ba concentrations (Sr_{aq} and Ba_{aq}) in solution were quantified using the ICP-MS ELAN 6100 DRC (PerkinElmer SCIEX) instrument. The filtered solution was diluted in 0.1 m HNO_3 by 1:1000 for Ba and 1:10,000 for Sr-measurements.

In addition to reference experiments with 0.1 mol/kg of NaCl, two sets of experiments were performed to investigate the influence of (1) elevated ionic strength and (2) Sr in the aqueous solution on the uptake of Ra during the recrystallization of barite:

1. Experiments with 1.0 mol/kg NaCl at 23 °C, 80 °C and 90 °C, (Table 1)
2. The concentration of Sr_{aq} was adjusted to either 0.05 mol/kg or 0.005 mol/kg. These concentrations were chosen such that the activity product $\{Sr^{2+}\}\{SO_4^{2-}\}$, as calculated with the GEM-Selector code [32,33], was close to or well below the solubility product of pure $SrSO_4$ (Table 2).

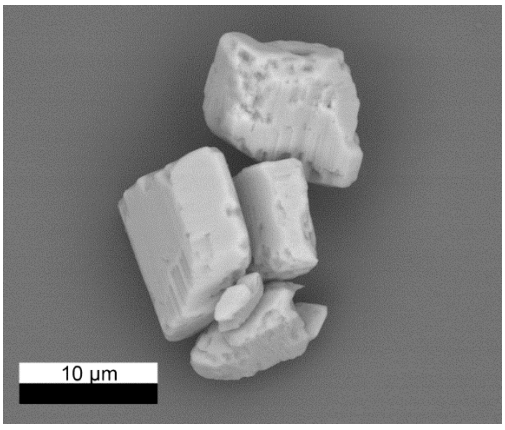

Figure 1. Scanning electron microscopy (SEM) image of initial barite particles before recrystallization experiments.

Table 1. Overview of experiments at elevated ionic strength.

Name	Ionic Strength	Solid/Liquid	Ra_{aq}	Temperature	Duration
	(mol/kg)	(g/kg)	(10^{-6} mol/kg)	(°C)	(days)
Reference 5 g/kg 1 mol/L NaCl RT	1	5	0	RT	951
Reference 0.5 g/kg 1 mol/L NaCl RT	1	0.5	0	RT	951
5 g/L 1 mol/kg NaCl RT	1	5	5	RT	951
0.5 g/L 1 mol/kg NaCl RT	1	0.5	5	RT	951
Reference 5 g/L 1 mol/kg NaCl 80	1	5	0	80	764
Reference 0.5 g/L 1 mol/kg NaCl 80	1	0.5	0	80	764
5 g/L 1 mol/kg NaCl 80	1	5	5	80	764
0.5 g/L 1 mol/kg NaCl 80	1	0.5	5	80	764
Reference 5 g/L 0.1 mol/kg NaCl 80	0.1	5	0	80	764
Reference 0.5 g/L 0.1 mol/kg NaCl 80	0.1	0.5	0	80	764
5 g/L 0.1 mol/kg NaCl 80	0.1	5	5	80	764
0.5 g/L 0.1 mol/kg NaCl 80	0.1	0.5	5	80	764
Reference 5 g/L 1 mol/kg NaCl 90	1	5	0	90	798
Reference 0.5 g/L 1 mol/kg NaCl 90	1	0.5	0	90	798
5 g/L 1 mol/kg NaCl 90	1	5	5	90	798
0.5 g/L 1 mol/kg NaCl 90	1	0.5	5	90	798

Table 2. Overview of experiments with Sr in the aqueous solution.

	Solid/Liquid	Ra_{aq}	Temperature	Sr_{aq}	Duration
	(g/kg)	(10^{-6} mol/kg)	(°C)	(mol/kg)	(days)
Reference 5 g/kg RT Sr 0.05	5	0	RT	0.05	683
Reference 5 g/kg RT Sr 0.005	5	0	RT	0.005	683
Reference 5 g/kg 90 Sr 0	5	0	90	0	1066
Reference 5 g/kg 90 Sr 0.05	5	0	90	0.05	1066
Reference 5 g/kg 90 Sr 0.005	5	0	90	0.005	1066
Reference 0.5 g/kg 90 Sr 0	0.5	0	90	0	1030
Reference 0.5 g/kg 90 Sr 0.05	0.5	0	90	0.05	1030
Reference 0.5 g/kg 90 Sr 0.005	0.5	0	90	0.005	1030
5 g/kg RT Sr 0.05_1	5	5	RT	0.05	683
5 g/kg RT Sr 0.005_1	5	5	RT	0.005	683
5 g/kg RT Sr 0.05_2	5	5	RT	0.05	683
5 g/kg Sr 0.005_2	5	5	RT	0.005	683
5 g/kg 90 Sr 0	5	5	90	0	1066
5 g/kg 90 Sr 0.05	5	5	90	0.05	1066
5 g/kg 90 Sr 0.005	5	5	90	0.005	1066
0.5 g/kg 90 Sr 0	0.5	5	90	0	1030
0.5 g/kg 90 Sr 0.05	0.5	5	90	0.05	1030
0.5 g/kg 90 Sr 0.005	0.5	5	90	0.005	1030

Small amounts of solid (10 µL of the suspension) were sampled during the recrystallization experiments. The evolution of the crystal morphology and chemical composition were studied using the environmental scanning electron microscope FEI Quanta 200 F (Eindhoven, Netherlands) combined with energy dispersive X-ray spectrometry (EDS, EDAX, Weiterstadt, Germany). In order to avoid artefacts due to precipitation of for example, NaCl, $SrSO_4$ or $RaSO_4$, the samples were separated from their solution by two washing steps in iso-propanol. The samples were then prepared as a suspension on a Cu or Si holder and subsequently dried.

Thermodynamic calculations for solid solution-aqueous solution systems (SS-AS) involve the calculation of the total equilibrium between the solid and the aqueous phase. Different to the case of single-phase equilibria, in which the solution composition is independent of the amount of solid, in the case of SS-AS not only the activities of ions in solution but also of the components of the solid need to be considered. In the case of a pure solid (e.g., barite) in water, the aqueous concentration for example, of Ba^{2+} for 0.5 or 5 g/kg H_2O at thermodynamic equilibrium will be the same. However, this is not the case for a solid solution for example, $(Ba,Ra)SO_4$. For SS-AS equilibria, the solution composition is linked to the composition of the solid. These equilibria were calculated assuming full equilibration of all barite and all cations in solution.

Gibbs energy minimization approaches implemented in the GEMS3K solver (http://gems.web.psi.ch/GEMS3K) and described in Kulik et al. (2013) [32] were used to calculate the solid solution composition as well as the aqueous solution equilibria at room temperature, 80 °C and 90 °C. The activity coefficients for all dissolved species (γ_j) are calculated according to the extended Debye-Hückel equation [34]. Equation (1) relates the activity coefficients of an aqueous ion to its charge (Z_j) and ionic strength (I) [33]:

$$log_{10}\gamma_j = \frac{-A_\gamma Z_j^2 \sqrt{I}}{1 + \dot{a} B_\gamma \sqrt{I}} + b_\gamma \, I \quad (1)$$

where $\dot{a}$ (in Å) is an average distance of approach of two ions of opposite charges, b_γ is a semi-empirical coefficient, either individual for a given electrolyte or common for all aqueous species. The parameters $\dot{a}$ and b_γ were set to 3.72 and 0.064, respectively, for all the ionic species [34]. A_γ and B_γ are temperature dependent coefficients obtained internally from SUPCRT92 subroutines [35] incorporated into the GEM3K code. At a temperature of 25 °C and pressure of 1 bar, the value of A_γ is approximately 0.5114 and B_γ is approximately 0.3288. Activity coefficients, γ_j for neutral species (dissolved gases) and water were set to unity.

Thermodynamic data for aqueous species were taken from the PSI-Nagra database [36] integrated in GEMS that inherits temperature and pressure dependencies for most aqueous ions and complexes from the HKF EoS [34] as given in the SUPCRT92 database (http://gems.web.psi.ch/TDB). Interaction parameters for the ternary (Ba,Sr,Ra)SO_4 solid-solution were taken from Klinkenberg et al. (2018) [22].

3. Results

3.1. Effect of Ionic Strength

The general evolution of the Ra concentrations in solution is similar as observed in earlier experiments [7,21]. All experimental data related to the effect of ionic strength are summarized in the appendix in Tables A1–A4. For comparison with the new data, experimental results from Brandt et al. (2015) [7] and Vinograd et al. (2018b) [21] are shown in Figure 2 and marked by § or *. At room temperature, the Ra-concentrations first reach minima of 7×10^{-8} mol/kg and 2×10^{-8} mol/kg in the experiments with S/L = 0.5 g/kg and 1.0 or 0.1 mol/kg of NaCl, respectively after 100–200 days. This minimum is then followed by a slight increase towards a plateau which represents a removal of 94% at high ionic strength and 99% of Ra at low ionic strength and S/L = 0.5 g/kg (Figure 2a). In the experiments with S/L = 0.5 g/kg, at higher temperatures the Ra-concentration slowly reaches a final plateau of the Ra-concentration and without going through the characteristic minimum observed at room temperature. The final concentration plateau systematically shifts to higher concentrations as a function of temperature which indicates less Ra uptake into the solid. In these experiments, the final Ra-concentration consistently stays lower for the experiments with lower ionic strength (Figure 2a,c,e) that is, the Ra-uptake capability of the barite decreases with increasing ionic strength.

At S/L = 5 g/kg the concentration plateau is at a similar level for all experiments with a Ra-concentration at around 10^{-8} mol/kg (Figure 2b,d,f). A strong effect of the S/L ratio regarding the kinetics of the Ra decrease is observed at all temperatures that is, higher S/L leads to a significantly higher uptake rate. The effect of ionic strength upon the kinetics of Ra uptake into barite is small in most of the experiments, except for the experiment at ambient conditions, 5 g/L of barite an 1.0 mol/kg of NaCl.

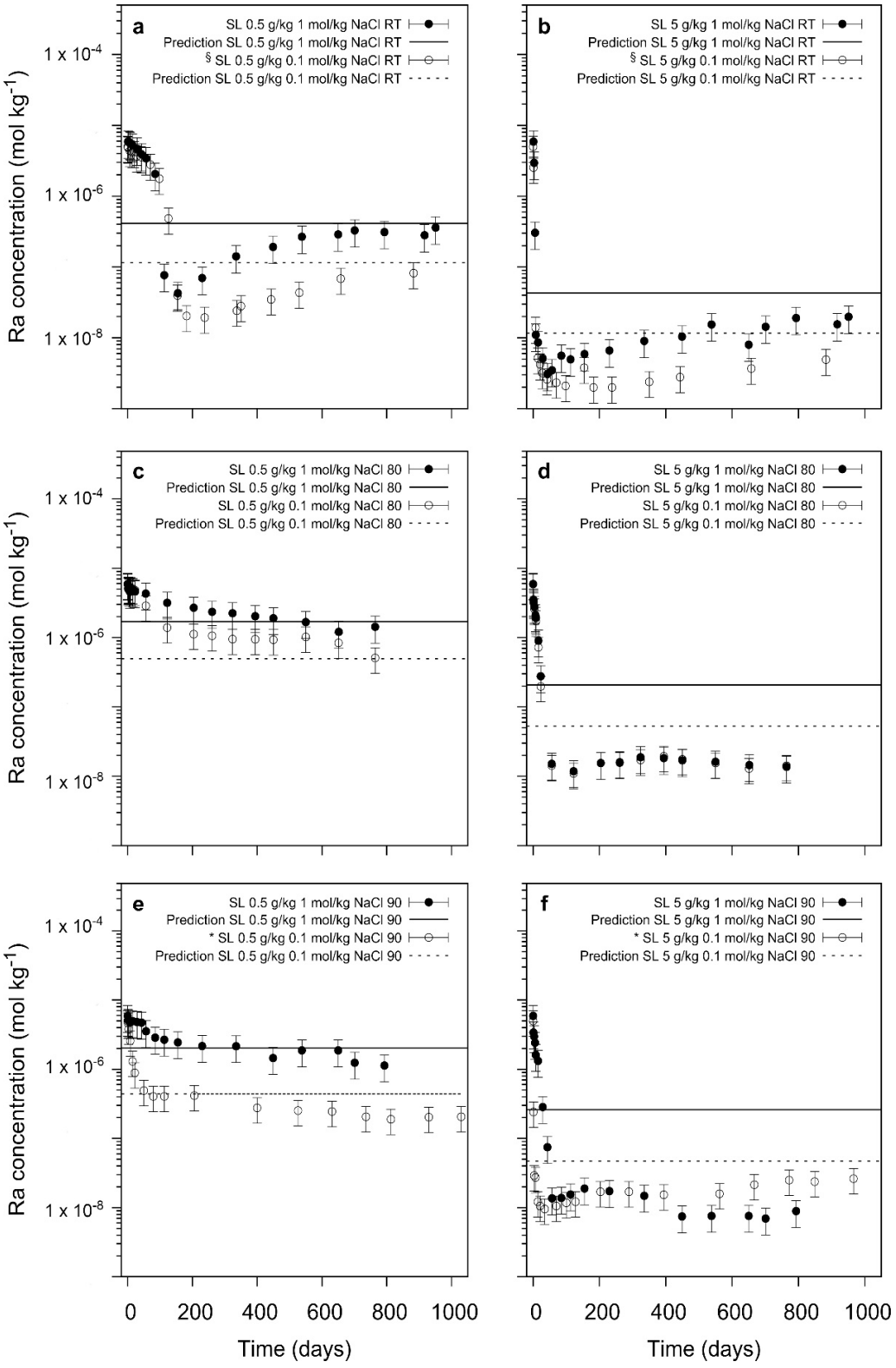

Figure 2. Temporal evolution of aqueous Ra_{aq} concentrations for experiments with an ionic strength of 1.0 mol/kg and 0.1 mol/kg of NaCl at ambient conditions (**a**,**b**) 80 °C (**c**,**d**) and 90 °C (**e**,**f**). Left column: experiments with a solid/liquid ratio of 0.5 g/kg, right column: 5 g/kg. The lines indicate predicted concentrations calculated by GEMS. Experimental data taken from Brandt et al., 2015 [7] marked §, experimental data from Vinograd et al., 2018b [21] marked with *.

3.2. Effect of Sr_{aq}

For comparison with the new data, data from experiments without Sr from Brandt et al. (2015) [7] and Vinograd et al. (2018b) [21] are shown in Figures 3 and 4 and marked by § or *. All experimental data related to the effect of Sr_{aq} are summarized in the appendix in Tables A5–A14. In experiments with S/L = 5 g/kg at room temperature and a low Sr_{aq} concentration of 0.005 mol/L (Figure 3b), the Ra_{aq} concentration decreased significantly within the first 300 days and reached a plateau of $4 \cdot 10^{-9}$ mol/kg. In contrast to the experiments at 90 °C, a kinetic effect of the presence of Sr is already noticeable at room temperature, 0.005 mol/kg Sr and high S/L = 5 g/kg (Figure 3b). Compared to the Ra-uptake experiment without Sr in solution (Figure 3a) the presence of Sr delays the Ra uptake. The final concentration plateau is reached after more than 200 days compared to less than one hundred days in the parallel Sr-free experiments. At higher Sr_{aq} concentration and room temperature almost no Ra uptake was measured even after almost 800 days of experimental time (S/L = 5 g/kg; Figure 3c). This corresponds to very stable Ba-concentrations in solution which are almost constant during all experiments with or without Ra, S/L = 5 g/kg at ambient conditions (Figure 4a–c).

Due to the expected retardation effect, a focus here was set on experiments at 90 °C. Compared to experiments without Sr in the aqueous solution [7,21], the uptake of Ra (Figure 3d–f) at 90 °C is affected already when only 0.05 mol/kg of Sr are present in solution. The inhibiting effect is present only slightly in the case of the experiment with a high S/L = 5 g/kg and clearly visible in the case of S/L = 0.5 g/kg (Figure 3e). While only the onset of the Ra-concentration plateau is delayed in the case of the higher S/L ratio, the presence of Sr clearly hinders the Ra-uptake in the lower S/L experiments. This leads to Ra concentrations decreasing slowly while in the Sr-free reference experiments the Ra concentration significantly decreases already during the first 100 days. This effect is even more pronounced in identical experiments at 90 °C but with 0.05 mol/kg of Sr (Figure 3f). Here, no significant Ra uptake could be observed even after more than 1000 days. In contrast, a significant uptake of Ra was still observed at S/L = 5 g/kg. A comparison of Ba-concentration data obtained for the experiments described above with data from parallel Ra-free reference experiments (Figure 4d–f) indicates only a minor effect of the presence of Ra and Sr in solution on the final Ba-concentration

In all experiments, no significant changes in the Sr_{aq} concentrations with time were observed. The values remained constant at 0.005 and 0.05 mol/kg, respectively (Figure 5a–d). All the experimental results of the aqueous metal ion concentrations are summarized in Tables A1–A14 of the Appendix A.

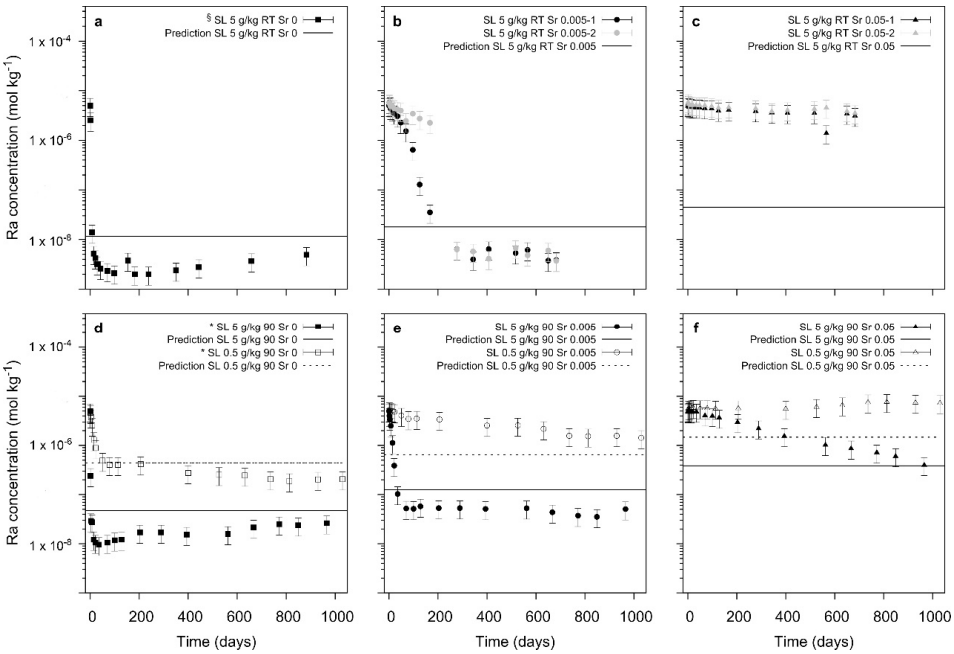

Figure 3. Temporal evolution of aqueous Ra_{aq} concentrations at ambient conditions (**a**–**c**) and 90 °C (**d**–**f**). Left column: experiments without Sr, middle column: experiments with 0.005 g/kg Sr and right column: experiments with 0.05 mol/kg Sr in the aqueous solution. The lines indicate predicted concentrations calculated by GEMS. Experimental data taken from Brandt et al., 2015 [7] marked §, experimental data from Vinograd et al., 2018b [21] marked with *.

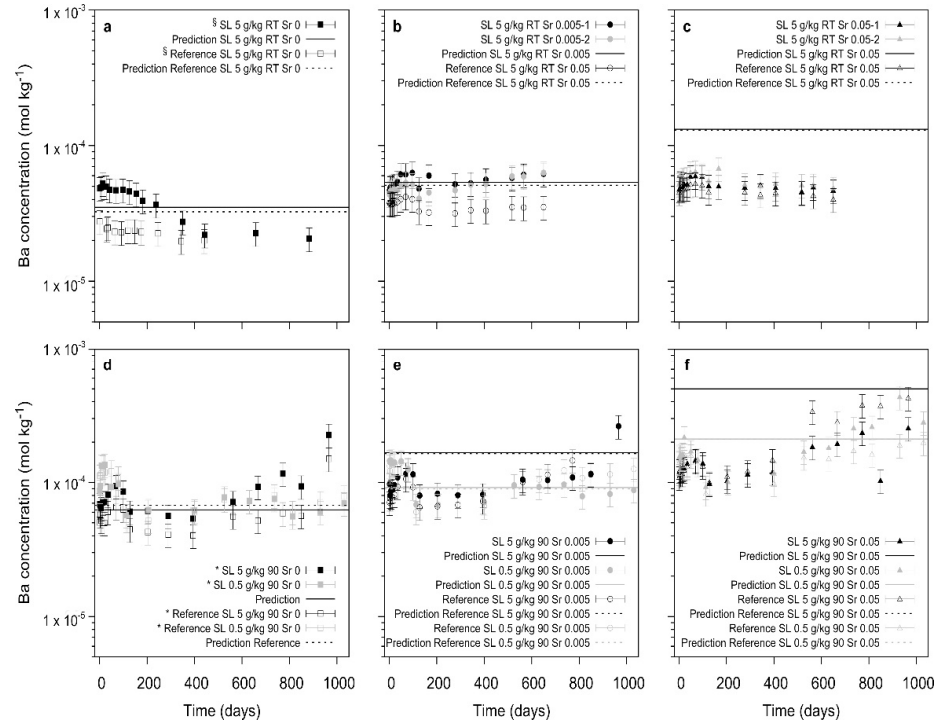

Figure 4. Temporal evolution of aqueous Ba_{aq} concentrations at ambient conditions (**a**–**c**) and 90 °C (**d**–**f**). Left column: experiments without Sr, middle column: experiments with 0.005 g/kg Sr and right column: experiments with 0.05 mol/kg Sr in the aqueous solution. The lines indicate predicted concentrations calculated by GEMS. Experimental data taken from Brandt et al., 2015 [7] marked §, experimental data from Vinograd et al., 2018b [21] marked with *.

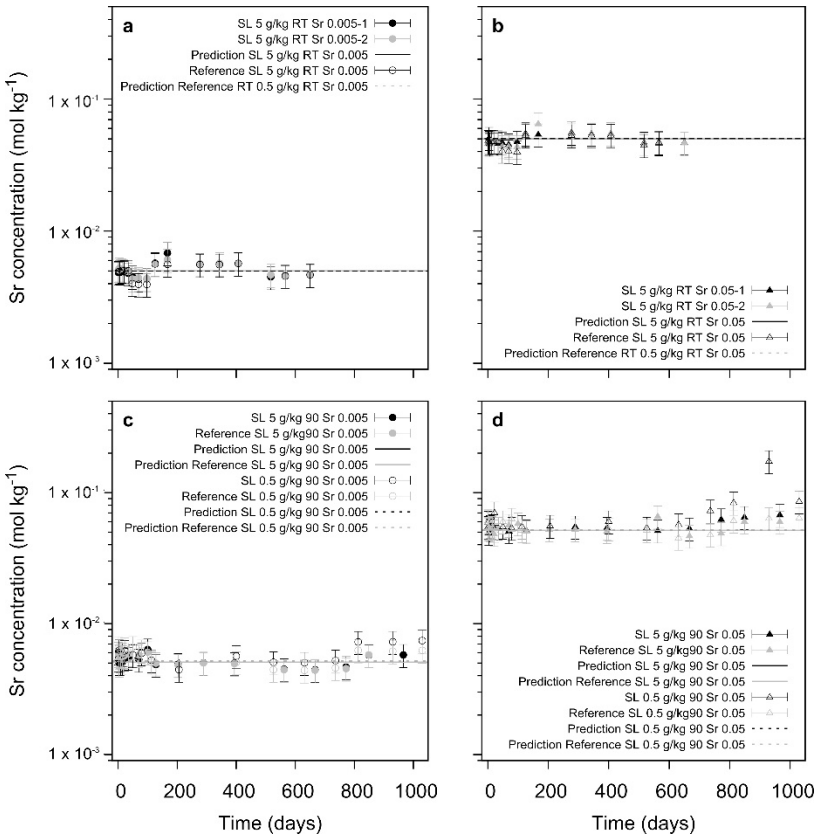

Figure 5. Temporal evolution of aqueous Sr_{aq} concentrations at room temperature (**a**,**b**) and 90 °C (**c**,**d**). Left column: experiments with 0.005 mol/kg Sr and right column: experiments with 0.05 mol/kg Sr in the aqueous solution. The lines indicate predicted concentrations calculated by GEMS.

3.3. Microstructural Evolution of the Solid

The general changes in the morphology of SL barite due to recrystallization are described in Klinkenberg et al. (2014) [10]. In difference to recent publications for example, Heberling et al. (2018) [5], in the preparation of the barite particles for our experiments the fines were removed and thus the grain size distribution narrowed to avoid Ostwald-ripening effects. Therefore, as in all our earlier experiments, only very slight surface effects were noted (Figures 6 and 7). No newly formed sulphate phases were observed in any of the experiments where Sr was added (Figure 7). In the experiments with 0.05 mol/kg Sr at ambient conditions and 90 °C, EDS confirmed uptake of Sr into the barite which was in a similar order of magnitude as predicted (3–4%) but a reliable quantification was difficult due to drying artefacts without sulphate on the surface. In all other experiments, no Sr could be detected by EDS. Ra was not detected in any solid by EDS indicating that only traces were taken up and/or that the uptake involves the barite particle's volume and not just the surface.

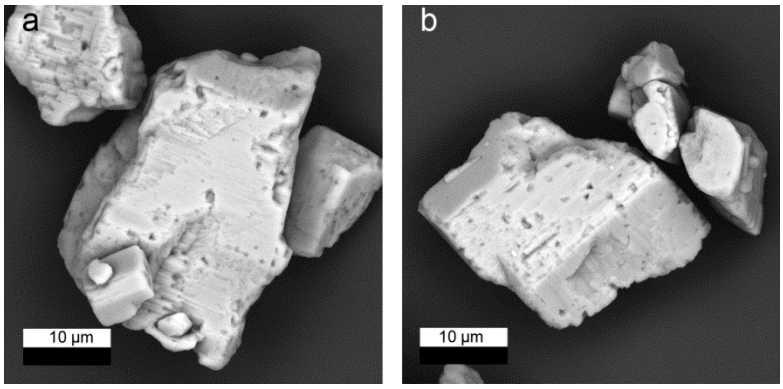

Figure 6. SEM micrographs of SL barite at the end of experiments with 1.0 mol/kg NaCl at 90 °C, (**a**) S/L = 5 g/kg, (**b**) 0.5 g/kg.

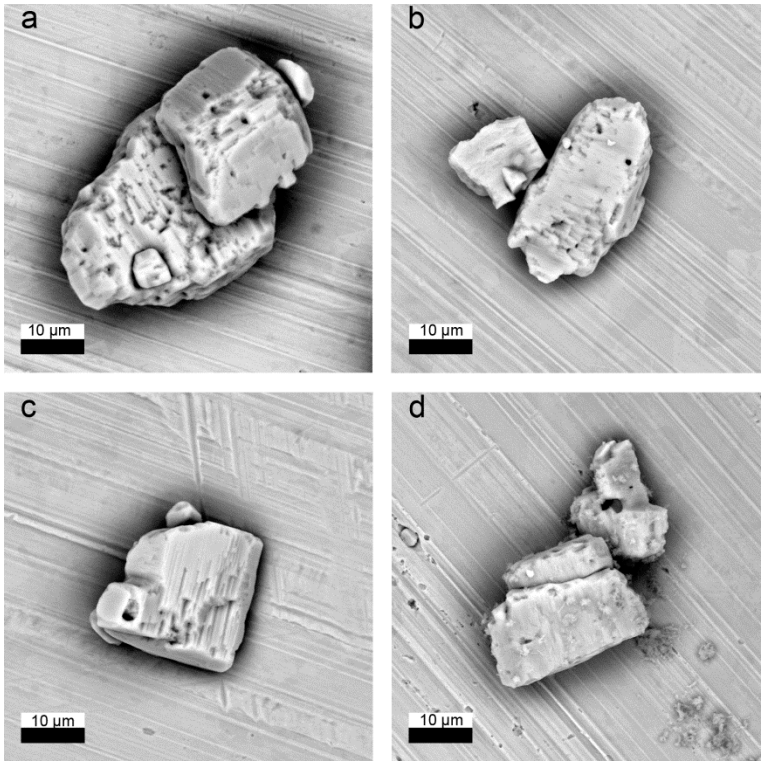

Figure 7. SEM micrographs of SL barite at the end of experiments with 0.005 mol/kg Sr (**a**,**c**) and 0.05 mol/kg Sr (**b**,**d**) in the aqueous solution at 90 °C. (**a**,**b**) S/L ratio = 5 g/kg, (**c**,**d**) S/L ratio = 0.5 g/kg.

EDS model calculations indicate that the adsorption or enrichment of Ra at the surface of the barite particles can be excluded because this would have created detectable concentrations of Ra at the particle surfaces. This is coherent with earlier studies by Klinkenberg et al. (2014) and Weber et al. (2017), Curti et al. (2010), [10,12,31] who all conclude upon structural uptake of Ra into the barite particles.

4. Discussion

4.1. Effect of Ionic Strength: Kinetics of Ra-Uptake and Approach to Equilibrium

The final Ra-concentrations of the recrystallization experiments at high ionic strength were compared with GEMS calculations which predict the full thermodynamic equilibrium of the respective solid solution-aqueous solution system. The calculated higher aqueous radium and barium concentration in solution for the high ionic strength experiment is explained by the increase in the

solubility of sulphates with increasing ionic strength [37,38]. For the experiments carried out with S/L = 0.5 g/kg, the relative difference between the low and high ionic strength as well as the final Ra-concentrations agree well with the thermodynamic predictions, indicating that the final state of the experiments is close to a full re-equilibration of the barite to a Ra-barite. In contrast, already at room temperature the experiments with S/L = 5 g/kg deviate from the predicted equilibrium. However, the results follow the predicted trend that is, the Ra-uptake is lower at high ionic strength. This trend diminishes at higher temperatures where the results at 0.1 mol/kg of NaCl and 1.0 mol/kg NaCl are very similar and far below the predicted concentrations. This effect at high S/L ratio has been observed earlier (e.g., [7,21]) and was attributed to entrapment effects which are later not re-equilibrated. Entrapment means that in addition to the amount of Ra taken up to fulfil the thermodynamic equilibrium, more Ra is "trapped" due to kinetic effects. Sometimes this may happen for example, as a result of overgrowth in areas where Ra is adsorbed to the surface. Entrapment is a kinetic effect and may be more visible at higher reaction rates. Compared to the experiments at S/L = 0.5 g/kg, the kinetics of recrystallization of the barite used in these experiments at S/L = 5 g/kg are much faster and may enable the uptake of additional Ra into barite due to such kinetic effects.

Zhang et al. (2014) [14] observed the effect of high ionic strength on the Ra-uptake during the co-precipitation of (Ba,Ra)SO_4. In contrast to their expectations the Ra-uptake was not lowered by ionic strength. Similar to the results presented in our study at high S/L ratio, the expected effect of lower Ra-uptake in Zhang et al. (2014) [14] was obscured by kinetic effects in Zhang et al. (2014) [14] as well.

4.2. Effect of Sr in Solution: Kinetics of Ra-Uptake and Approach to Equilibrium

Previous studies on the co-precipitation of radium with barite in the presence of strontium indicated a strong impact of the supersaturation on the effect of Sr on crystal growth of barite. Ceccarello et al. (2004) [24] studied the diffusion-controlled growth of (Ba,Sr)SO_4. They noticed that the uptake of Ra only happened during the nucleation phase and that this uptake decreased with increasing Sr in the mother solutions. Consistently, Zhang et al. (2014) [14] noted only very little impact of the presence of Sr on the Ra-uptake during co-precipitation. In addition, studies on the removal of Sr by barite precipitation have shown that the effect of ionic strength and competitive ions (Ca^{2+} and Mg^{2+}) can be neglected at higher supersaturation [39]. Recent studies on crystal growth of barite in the presence of Sr_{aq} at low supersaturation indicate important implications of the Sr/Ba-ratio in solution on barite growth [40–42]. These studies described the inhibiting effect of strontium on barite growth observed in our study. At elevated temperatures of 108 °C, Weber et al. (2018) [41] observed that at low Sr/Ba ratios (<5.5) in the solution Sr_{aq} is inhibiting barite crystal growth. In contrast, at higher aqueous Sr/Ba ratios the inhibiting effect of strontium on barite growth is overcome by a shift in the growth mechanism from typical barite growth to celestine growth.

In contrast to the studies at high supersaturation discussed above, in the present study, the recrystallization of barite and uptake of Ra requires a continuous dissolution and growth of barite at close to equilibrium conditions. Previous microstructural analyses have shown that the highly porous microstructure of the same barite as used in the recrystallization experiments presented here supports the recrystallization process in addition to the chemical disequilibrium with the solution [11,12,43]. Because we use the same barite starting material in our study, a similar radium uptake mechanism via a dissolution and re-precipitation mechanism is expected. The concentration of Sr_{aq} present in solution is orders of magnitude higher compared to the Ba_{aq} throughout the whole evolution of the experiment (Figures 4 and 5), despite Ba being released into the solution by dissolution of the original barite particles. We therefore formulate the hypothesis that there is not sufficient Ba present in the solution to compensate for the elevated strontium concentration. Therefore, it appears likely that the presence of Sr affects the recrystallization process of barite and can only be accommodated properly to form a ternary solid-solution at elevated temperatures and/or high S/L ratios. At all temperatures and low Sr-concentrations, the effect of Sr upon the Ra-uptake into barite is small. This can be observed in

the final Ra_{aq}-concentrations, which at high S/L = 5 g/kg, are close or slightly below the predicted values (Figure 3a,b,d,e). In general, the kinetics at high S/L are much faster than at low S/L which further strengthens our hypothesis that the Ba released during the recrystallization is needed to compensate for the higher Sr concentration in the solution. Therefore, the impact of Sr is overcome by the general kinetics of the recrystallization at high S/L ratios. However, at room temperature and high Sr-concentrations or at low S/L and 90 °C where the kinetics in the reference system are already slow, a significant impact of the presence of Sr is noted. Here, the recrystallization process appears to be poisoned by the presence of Sr (Figure 3c,f).

The total amount of sulphate within the system is too low to accommodate all Sr and Ba in the solid that is, during the re-equilibration. Therefore, an exchange between Sr and Ba is needed. Thermodynamic calculations predict more Ba to be soluble in our fully equilibrated systems after the uptake of Sr and Ra than in equilibrium with pure barite. In addition, Sr competes with Ra in solution.

Recent studies using in situ resonant anomalous X-ray reflectivity (RAXR) in combination with density functional theory (DFT) and classical molecular dynamics (CMD) showed the adsorption of Sr as inner-sphere complexes and the incorporation into the outermost barite layers [44]. The free energy landscape for metal adsorption of Sr^{2+} indicated distinct inner-sphere sites with additional outer-sphere sites which are energetically less favourable. In particular, the energy barrier for Sr^{2+} was observed to be lower than for Ba^{2+} which indicates a fast exchange among the adsorbed Sr^{2+} species [44]. Based on these results, it is most likely that the presence of high Sr_{aq} concentrations is unfavourable for Ra-uptake because here the competition between Ra and Sr in solution for sulphate binding sites is won by Sr. In fact, at room temperature, in our experiments Sr appears not to be forming the solid-solution with $BaSO_4$ which is thermodynamically predicted but is only adsorbed to the surface, as indicated by the Ba concentration in solution much lower than expected in equilibrium. At 0.05 mol/kg of Sr_{aq}, the surplus of Sr may be so high that more or all Ba sites at the surface are exchanged for Sr, thus stopping the recrystallization of barite completely. In all other cases, the final concentrations of Ba, Ra and Sr are close to the thermodynamically predicted levels.

5. Conclusions

In this study, the kinetics and thermodynamic aspects of the presence of ions in solution upon the uptake of ^{226}Ra during the recrystallization of barite was studied with variation of temperature. In contrast to earlier studies which were dominated by nucleation processes and crystal growth at high supersaturation, the ^{226}Ra-uptake during barite recrystallization is a process at close-to-equilibrium conditions. This process is kinetically not very much affected by the increase of ionic strength from 0.1 mol/kg of NaCl to 1.0 mol/kg. The increase of ionic strength from 0.1 to 1.0 mol/kg of NaCl slightly decreases the retention potential of barite, following the trend predicted by thermodynamic model calculations for the experiments at low solid/liquid ratio. At higher S/L, this trend is only observed at ambient temperatures whereas at higher temperatures kinetic effects appear to lead to an additional uptake of Ra—leading to very similar results at both ionic strengths.

The specific interaction of Sr_{aq} with the recrystallizing barite and ^{226}Ra leads to a significant decrease in the ^{226}Ra uptake. At low S/L ratio and at ambient conditions, even after 800 to 1000 days the uptake process appears to be inhibited by the presence of Sr_{aq}, indicating a poisoning of the barite surfaces by adsorbed Sr. In the cases where barite is able to recrystallize, thermodynamically predicted trends of the final Ra-concentrations are confirmed. In contrast to earlier studies where $SrSO_4$ was present in the solid phase, the addition of Sr in solution leads to a competition of Sr with Ba and Ra during the recrystallization process. At slow recrystallization kinetics due to a low S/L ratio and/or low temperature, a significant effect of Sr_{aq} is noted which at the extreme point appears to inhibit the complete barite recrystallization and also the Ra-uptake.

In summary, the unspecific effect of ionic strength has only little consequence upon the Ra-uptake during barite recrystallization whereas Sr in solution appears to stop this process at certain conditions (Figure 8).

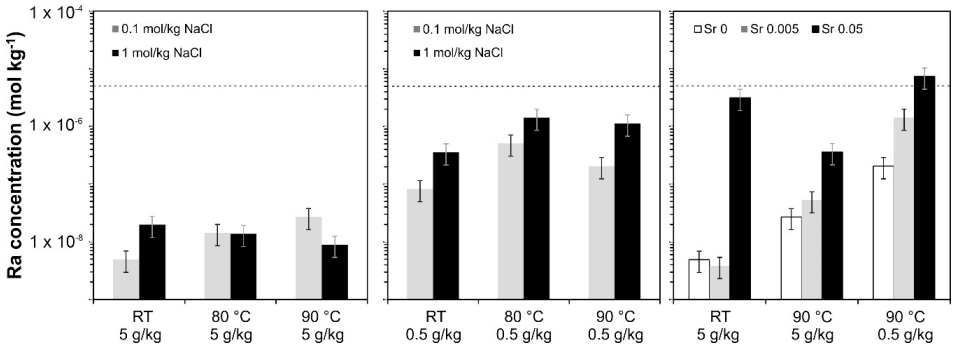

Figure 8. Ra_{aq} concentrations at the end of experiments. The dashed lines indicate the starting concentrations of Ra_{aq}.

Author Contributions: F.B. conceived and designed the experiments and prepared and finalized the paper draft. M.K. carried out part of the recrystallization experiments and the treatment of all data as well as electron microscopy and developed all figures, J.P. performed all thermodynamic calculations and their interpretation, J.W. set up some recrystallization experiments, performed part of the electron microscopy and their data treatment, D.B. finalized the paper along with all co-authors. All authors contributed to writing the manuscript.

Funding: The research leading to these results has received partial funding from the German Federal Ministry of Education and Research (BMBF) ImmoRad project (project number 02NUK019C) and ThermAc project (project number 02NUK039D).

Acknowledgments: We are grateful to F. Sadowski, K. Dahmen, A. Wilden, R. König and G. Modolo for their support. The authors would also like to thank five anonymous reviewers for their careful and constructive reviews which improved this publication.

Conflicts of Interest: The authors declare no conflict of interest.

Appendix A

Table A1. Ra concentrations of experiments with 1.0 mol/kg NaCl at room temperature.

	Ra Concentration (mol/kg)	
Name	**5 g/kg 1 mol/kg NaCl RT**	**0.5 g/kg 1 mol/kg NaCl RT**
Day		
0	5.90×10^{-6}	5.90×10^{-6}
1	2.95×10^{-6}	5.90×10^{-6}
3	3.04×10^{-7}	5.72×10^{-6}
6	1.10×10^{-8}	5.53×10^{-6}
8	8.59×10^{-9}	5.29×10^{-6}
15	5.11×10^{-9}	4.69×10^{-6}
29	3.07×10^{-9}	3.90×10^{-6}
43	3.07×10^{-9}	3.42×10^{-6}
57	5.58×10^{-9}	2.06×10^{-6}
85	4.95×10^{-9}	7.67×10^{-8}
113	5.89×10^{-9}	4.27×10^{-8}
155	6.61×10^{-9}	6.99×10^{-8}
230	9.00×10^{-9}	1.41×10^{-7}
335	1.04×10^{-8}	1.92×10^{-7}
449	1.54×10^{-8}	2.67×10^{-7}
538	7.98×10^{-9}	2.88×10^{-7}
650	1.43×10^{-8}	3.28×10^{-7}
701	1.90×10^{-8}	3.11×10^{-7}
793	1.55×10^{-8}	2.81×10^{-7}
917	1.98×10^{-8}	3.60×10^{-7}
951	1.97×10^{-8}	3.58×10^{-7}

Table A2. Ra concentrations of experiments with 1.0 mol/kg NaCl at 80 °C.

	Ra Concentration (mol/kg)	
Name	**5 g/kg 1 mol/kg NaCl 80**	**0.5 g/kg 1 mol/kg NaCl 80**
Day		
0	5.90×10^{-6}	5.90×10^{-6}
1	3.52×10^{-6}	5.09×10^{-6}
2	3.33×10^{-6}	5.22×10^{-6}
4	2.78×10^{-6}	4.83×10^{-6}
7	2.10×10^{-6}	4.56×10^{-6}
9	1.92×10^{-6}	5.07×10^{-6}
16	9.01×10^{-7}	4.81×10^{-6}
23	2.77×10^{-7}	4.62×10^{-6}
56	1.51×10^{-8}	4.30×10^{-6}
122	1.18×10^{-8}	3.17×10^{-6}
204	1.55×10^{-8}	2.69×10^{-6}
261	1.59×10^{-8}	2.35×10^{-6}
324	1.88×10^{-8}	2.24×10^{-6}
394	1.83×10^{-8}	2.03×10^{-6}
450	1.70×10^{-8}	1.90×10^{-6}
550	1.62×10^{-8}	1.67×10^{-6}
652	1.45×10^{-8}	1.21×10^{-6}
764	1.37×10^{-8}	1.43×10^{-6}

Table A3. Ra concentrations of experiments with 0.1 mol/kg NaCl at 80 °C.

	Ra Concentration (mol/kg)	
Name	**5 g/kg 0.1 mol/kg NaCl 80**	**0.5 g/kg 0.1 mol/kg NaCl 80**
Day		
0	5.90×10^{-6}	
1	3.28×10^{-6}	5.88×10^{-6}
2	3.13×10^{-6}	5.19×10^{-6}
3		5.04×10^{-6}
4	2.57×10^{-6}	5.13×10^{-6}
7	1.95×10^{-6}	5.18×10^{-6}
9	1.73×10^{-6}	5.25×10^{-6}
16	7.23×10^{-7}	5.07×10^{-6}
23	1.97×10^{-7}	4.78×10^{-6}
56	1.43×10^{-8}	2.87×10^{-6}
122	1.10×10^{-8}	1.39×10^{-6}
204		1.12×10^{-6}
261	1.57×10^{-8}	1.06×10^{-6}
324	1.72×10^{-8}	9.48×10^{-7}
394	1.94×10^{-8}	9.45×10^{-7}
450	1.76×10^{-8}	9.31×10^{-7}
550	1.55×10^{-8}	1.02×10^{-6}
651	1.29×10^{-8}	8.38×10^{-7}
764	1.42×10^{-8}	5.08×10^{-7}

Table A4. Ra concentrations of experiments with 1.0 mol/kg NaCl at 90 °C.

	Ra Concentration (mol/kg)	
Name	**5 g/kg 1 mol/kg NaCl 90**	**0.5 g/kg 1 mol/kg NaCl 90**
Day		
0	5.90×10^{-6}	5.90×10^{-6}
1	3.39×10^{-6}	5.15×10^{-6}
3	2.98×10^{-6}	5.10×10^{-6}
6	2.41×10^{-6}	4.86×10^{-6}
8	1.61×10^{-6}	4.75×10^{-6}
15	1.32×10^{-6}	4.97×10^{-6}
29	2.84×10^{-7}	4.81×10^{-6}
43	7.47×10^{-8}	4.71×10^{-6}
57	1.36×10^{-8}	3.54×10^{-6}
85	1.38×10^{-8}	2.86×10^{-6}
113	1.55×10^{-8}	2.67×10^{-6}
155	1.89×10^{-8}	2.44×10^{-6}
230	1.73×10^{-8}	2.16×10^{-6}
335	1.48×10^{-8}	2.15×10^{-6}
449	7.44×10^{-9}	1.45×10^{-6}
538	7.57×10^{-9}	1.87×10^{-6}
650	7.57×10^{-9}	1.87×10^{-6}
701	6.95×10^{-9}	1.24×10^{-6}
793	8.90×10^{-9}	1.13×10^{-6}

Table A5. Ra concentration of experiments with Sr in the aqueous solution at 90 °C.

	Ra Concentration (mol/kg)						
Day	**SL 5 g/kg 90 Sr 0**	**SL 5 g/kg 90 Sr 0.05**	**SL 5 g/kg 90 Sr 0.005**	**Day**	**SL 0.5 g/kg 90 Sr 0**	**SL 0.5 g/kg 90 Sr 0.05**	**SL 0.5 g/kg 90 Sr 0.005**
1	2.41×10^{-7}	4.84×10^{-6}	4.02×10	1	4.64×10^{-6}	5.62×10^{-6}	5.25×10^{-6}
3	2.90×10^{-8}	5.08×10^{-6}	3.39×10^{-6}	3	3.78×10^{-6}	5.59×10^{-6}	5.21×10^{-6}
7	2.72×10^{-8}	5.06×10^{-6}	2.51×10^{-6}	8	2.57×10^{-6}	5.47×10^{-6}	5.05×10^{-6}
14	1.21×10^{-8}	4.81×10^{-6}	1.13×10^{-6}	15	1.30×10^{-6}	5.81×10^{-6}	4.99×10^{-6}
21	1.05×10^{-8}	4.89×10^{-6}	3.88×10^{-7}	22	8.88×10^{-7}	5.88×10^{-6}	4.83×10^{-6}
35	9.55×10^{-9}	4.93×10^{-6}	1.03×10^{-7}	50	4.92×10^{-7}	5.80×10^{-6}	4.06×10^{-6}
70	1.05×10^{-8}	4.13×10^{-6}	5.21×10^{-8}	79	4.04×10^{-7}	5.80×10^{-6}	3.46×10^{-6}
100	1.17×10^{-8}	4.03×10^{-6}	5.13×10^{-8}	113	4.04×10^{-7}	5.68×10^{-6}	3.52×10^{-6}
128	1.21×10^{-8}	3.72×10^{-6}	5.75×10^{-8}	206	4.16×10^{-7}	5.76×10^{-6}	3.37×10^{-6}
203	1.70×10^{-8}	3.02×10^{-6}	5.30×10^{-8}	400	2.76×10^{-7}	5.63×10^{-6}	2.54×10^{-6}
289	1.70×10^{-8}	2.25×10^{-6}	5.30×10^{-8}	526	2.53×10^{-7}	6.14×10^{-6}	2.56×10^{-6}
394	1.53×10^{-8}	1.57×10^{-6}	5.11×10^{-8}	631	2.45×10^{-7}	6.65×10^{-6}	2.17×10^{-6}
562	1.59×10^{-8}	1.04×10^{-6}	5.28×10^{-8}	736	2.06×10^{-7}	7.62×10^{-6}	1.57×10^{-6}
667	2.14×10^{-8}	8.78×10^{-7}	4.36×10^{-8}	813	1.89×10^{-7}	7.76×10^{-6}	1.54×10^{-6}
772	2.50×10^{-8}	7.28×10^{-7}	3.72×10^{-8}	930	2.03×10^{-7}	7.53×10^{-6}	1.57×10^{-6}
849	2.37×10^{-8}	6.11×10^{-7}	3.52×10^{-8}	1030	2.06×10^{-7}	7.39×10^{-6}	1.43×10^{-6}
966	2.62×10^{-8}	4.04×10^{-7}	5.07×10^{-8}				
1066	2.70×10^{-8}	3.61×10^{-7}	5.30×10^{-8}				

Table A6. Sr concentration of experiments with Sr in the aqueous solution at 90 °C.

Sr Concentration (mol/kg)					
Day	**SL 5 g/kg 90 Sr 0.05**	**SL 5 g/kg 90 Sr 0.005**	**Day**	**SL 0.5 g/kg 90 Sr 0.05**	**SL 0.5 g/kg 90 Sr 0.005**
1	5.49×10^{-2}	6.03×10^{-3}	1	5.98×10^{-2}	5.35×10^{-3}
3	5.46×10^{-2}	5.02×10^{-3}	3	4.94×10^{-2}	6.25×10^{-3}
7	5.23×10^{-2}	5.28×10^{-3}	8	5.56×10^{-2}	5.00×10^{-3}
14	5.52×10^{-2}	5.06×10^{-3}	15	5.64×10^{-2}	5.87×10^{-3}
21	5.40×10^{-2}	5.40×10^{-3}	22	7.05×10^{-2}	6.17×10^{-3}
35	5.41×10^{-2}	5.49×10^{-3}	50	5.51×10^{-2}	5.74×10^{-3}
70	5.11×10^{-2}	5.31×10^{-3}	79	5.40×10^{-2}	5.93×10^{-3}
100	5.82×10^{-2}	6.35×10^{-3}	113	5.54×10^{-2}	5.25×10^{-3}
128	5.14×10^{-2}	4.86×10^{-3}	206	5.59×10^{-2}	4.45×10^{-3}
203	5.23×10^{-2}	4.90×10^{-3}	400	6.04×10^{-2}	5.65×10^{-3}
289	5.51×10^{-2}	5.03×10^{-3}	519	5.41×10^{-2}	5.06×10^{-3}
394	5.39×10^{-2}	5.00×10^{-3}	631	5.73×10^{-2}	5.02×10^{-3}
562	5.14×10^{-2}	4.49×10^{-3}	736	7.30×10^{-2}	5.22×10^{-3}
667	5.33×10^{-2}	4.45×10^{-3}	813	8.40×10^{-2}	7.24×10^{-3}
772	6.26×10^{-2}	4.66×10^{-3}	930	1.74×10^{-1}	7.26×10^{-3}
849	6.52×10^{-2}	5.74×10^{-3}	1030	8.59×10^{-2}	7.41×10^{-3}
966	6.77×10^{-2}	5.77×10^{-3}			
1066	6.58×10^{-2}	5.73×10^{-3}			

Table A7. Sr concentration of Reference experiments with Sr in the aqueous solution at 90 °C.

Sr Concentration Reference without Ra (mol/kg)					
Day	**Reference SL 5 g/kg 90 Sr 0.05**	**Reference SL 5 g/kg 90 Sr 0.005**	**Day**	**Reference SL 0.5 g/kg 90 Sr 0.05**	**Reference SL 0.5 g/kg 90 Sr 0.005**
1	5.37×10^{-2}	5.76×10^{-3}	1	6.16×10^{-2}	6.62×10^{-3}
3	5.33×10^{-2}	5.61×10^{-3}	3	5.37×10^{-2}	4.87×10^{-3}
7	5.55×10^{-2}	5.68×10^{-3}	8	5.90×10^{-2}	5.67×10^{-3}
14	5.43×10^{-2}	5.62×10^{-3}	15	5.49×10^{-2}	5.68×10^{-3}
21	4.85×10^{-2}	5.68×10^{-3}	22	5.15×10^{-2}	6.45×10^{-3}
35	5.39×10^{-2}	5.86×10^{-3}	50	6.04×10^{-2}	6.63×10^{-3}
70	5.68×10^{-2}	5.74×10^{-3}	79	6.32×10^{-2}	6.24×10^{-3}
100	5.82×10^{-2}	6.05×10^{-3}	113	5.19×10^{-2}	5.06×10^{-3}
128	5.08×10^{-2}	4.98×10^{-3}	206		
203	5.23×10^{-2}	4.83×10^{-3}	400	5.34×10^{-2}	5.07×10^{-3}
289	5.26×10^{-2}	5.00×10^{-3}	519	5.20×10^{-2}	4.45×10^{-3}
394	5.10×10^{-2}	4.94×10^{-3}	631	4.53×10^{-2}	4.39×10^{-3}
562	6.59×10^{-2}	4.44×10^{-3}	736	4.78×10^{-2}	4.59×10^{-3}
667	4.69×10^{-2}	4.40×10^{-3}	813	6.13×10^{-2}	6.25×10^{-3}
772	4.91×10^{-2}	4.53×10^{-3}	930	6.39×10^{-2}	6.15×10^{-3}
849	6.05×10^{-2}	5.77×10^{-3}	1030	6.41×10^{-2}	6.23×10^{-3}
966	6.02×10^{-2}	4.93×10^{-3}			
1066	6.24×10^{-2}	5.11×10^{-3}			

Table A8. Ba concentration of experiments with Sr in the aqueous solution at 90 °C.

	Ba Concentration (mol/kg)						
Day	**SL 5 g/kg 90 Sr 0**	**SL 5 g/kg 90 Sr 0.05**	**SL 5 g/kg 90 Sr 0.005**	**Day**	**SL 0.5 g/kg 90 Sr 0**	**SL 0.5 g/kg 90 Sr 0.05**	**SL 0.5 g/kg 90 Sr 0.005**
1	6.90×10^{-5}	1.19×10^{-4}	9.73×10^{-5}	1	8.66×10^{-5}	1.54×10^{-4}	1.45×10^{-4}
3	6.74×10^{-5}	1.23×10^{-4}	8.02×10^{-5}	3	9.38×10^{-5}	1.58×10^{-4}	1.42×10^{-4}
7	6.46×10^{-5}	1.25×10^{-4}	8.67×10^{-5}	8	1.33×10^{-4}	1.60×10^{-4}	1.46×10^{-4}
14	7.07×10^{-5}	1.27×10^{-4}	8.83×10^{-5}	15	1.32×10^{-4}	1.63×10^{-4}	1.39×10^{-4}
21	7.15×10^{-5}	1.28×10^{-4}	9.56×10^{-5}	22	1.35×10^{-4}	2.17×10^{-4}	1.41×10^{-4}
35	8.08×10^{-5}	1.38×10^{-4}	1.09×10^{-4}	50	9.23×10^{-5}	1.71×10^{-4}	1.44×10^{-4}
70	9.42×10^{-5}	1.47×10^{-4}	1.16×10^{-4}	79	9.73×10^{-5}	1.48×10^{-4}	1.25×10^{-4}
100	8.56×10^{-5}	1.39×10^{-4}	1.15×10^{-4}	113	5.70×10^{-5}	9.30×10^{-4}	6.83×10^{-5}
128	6.06×10^{-5}	9.79×10^{-5}	7.99×10^{-5}	206	6.23×10^{-5}	1.01×10^{-4}	6.79×10^{-5}
203	6.14×10^{-5}	1.03×10^{-4}	8.25×10^{-5}	400	6.17×10^{-5}	1.17×10^{-4}	7.13×10^{-5}
289	5.62×10^{-5}	1.15×10^{-4}	8.03×10^{-5}	519	7.74×10^{-5}	1.70×10^{-4}	9.48×10^{-5}
394	5.37×10^{-5}	1.19×10^{-4}	8.15×10^{-5}	631	7.31×10^{-5}	1.81×10^{-4}	9.27×10^{-5}
562	7.15×10^{-5}	1.84×10^{-4}	1.05×10^{-4}	736	7.54×10^{-5}	2.54×10^{-4}	9.64×10^{-5}
667	9.29×10^{-5}	1.94×10^{-4}	1.04×10^{-4}	813	5.59×10^{-5}	2.60×10^{-4}	7.89×10^{-5}
772	1.16×10^{-4}	2.35×10^{-4}	1.09×10^{-4}	930	6.05×10^{-5}	4.34×10^{-4}	8.21×10^{-5}
849	9.35×10^{-5}	1.03×10^{-4}	1.16×10^{-4}	1030	6.99×10^{-5}	2.81×10^{-4}	8.78×10^{-5}
966	2.27×10^{-4}	2.54×10^{-4}	2.63×10^{-4}				
1066	8.93×10^{-5}	1.42×10^{-4}	1.62×10^{-4}				

Table A9. Ba concentration of Reference experiments with Sr in the aqueous solution of at 90 °C.

	Ba Concentration Reference without Ra (mol/kg)						
Day	**Reference SL 5 g/kg 90 Sr 0**	**Reference SL 5 g/kg 90 Sr 0.05**	**Reference SL 5 g/kg 90 Sr 0.005**	**Day**	**Reference SL 0.5 g/kg 90 Sr 0**	**Reference SL 0.5 g/kg 90 Sr 0.05**	**Reference SL 0.5 g/kg 90 Sr 0.005**
1	5.03×10^{-5}	1.09×10^{-4}	7.09×10^{-5}	1	1.12×10^{-4}	1.41×10^{-4}	1.33×10^{-4}
3	5.73×10^{-5}	1.13×10^{-4}	7.64×10^{-5}	3	1.13×10^{-4}	1.44×10^{-4}	1.22×10^{-4}
7	5.19×10^{-5}	1.16×10^{-4}	7.90×10^{-5}	8	1.16×10^{-4}	1.51×10^{-4}	1.38×10^{-4}
14	5.01×10^{-5}	1.16×10^{-4}	7.74×10^{-5}	15	1.19×10^{-4}	1.53×10^{-4}	1.36×10^{-4}
21	5.00×10^{-5}	1.23×10^{-4}	8.12×10^{-5}	22	1.19×10^{-4}	1.61×10^{-4}	1.36×10^{-4}
35	6.04×10^{-5}	1.31×10^{-4}	9.31×10^{-5}	50	1.21×10^{-4}	1.59×10^{-4}	1.41×10^{-4}
70	6.57×10^{-5}	1.44×10^{-4}	1.06×10^{-4}	79	1.09×10^{-4}	1.38×10^{-4}	1.27×10^{-4}
100	6.30×10^{-5}	1.32×10^{-4}	9.21×10^{-5}	113	5.27×10^{-5}	8.28×10^{-5}	6.03×10^{-5}
128	4.46×10^{-5}	1.00×10^{-4}	6.51×10^{-5}	206	5.20×10^{-5}		
203	4.27×10^{-5}	1.11×10^{-4}	6.65×10^{-5}	400	6.01×10^{-5}	9.83×10^{-5}	6.65×10^{-5}
289	4.09×10^{-5}	1.21×10^{-4}	6.79×10^{-5}	519	7.46×10^{-5}	1.54×10^{-4}	9.55×10^{-5}
394	4.02×10^{-5}	1.47×10^{-4}	7.24×10^{-5}	631	7.27×10^{-5}	1.50×10^{-4}	1.05×10^{-4}
562	5.59×10^{-5}	3.38×10^{-4}	1.01×10^{-4}	736	8.01×10^{-5}	1.72×10^{-4}	1.23×10^{-4}
667	5.19×10^{-5}	2.82×10^{-4}	1.14×10^{-4}	849	6.03×10^{-5}	1.62×10^{-4}	1.08×10^{-4}
772	5.90×10^{-5}	3.77×10^{-4}	1.46×10^{-4}	966	7.11×10^{-5}	1.90×10^{-4}	1.15×10^{-4}
849	5.65×10^{-5}	3.73×10^{-4}	1.15×10^{-4}	1066	7.86×10^{-5}	1.98×10^{-4}	1.26×10^{-4}
966	1.50×10^{-4}	4.27×10^{-4}					
1066	1.36×10^{-4}	4.52×10^{-4}					

Table A10. Ra concentration of experiments with Sr in the aqueous solution at 23 °C.

	Ra Concentration (mol/kg)			
Day	**SL 5 g/kg RT Sr 0.05_1**	**SL 0.5 g/kg RT Sr 0.005_1**	**SL 5 g/kg RT Sr 0.05_2**	**SL 5 g/kg RT Sr 0.005_2**
1	5.41×10^{-6}	5.79×10^{-6}	5.94×10^{-6}	5.70×10^{-6}
4	4.90×10^{-6}	5.12×10^{-6}	5.46×10^{-6}	5.23×10^{-6}
6	4.75×10^{-6}	4.40×10^{-6}	5.39×10^{-6}	4.87×10^{-6}
13	4.75×10^{-6}	4.06×10^{-6}	5.16×10^{-6}	4.85×10^{-6}
20	4.68×10^{-6}	3.49×10^{-6}	5.23×10^{-6}	4.46×10^{-6}
34	4.63×10^{-6}	3.06×10^{-6}	5.18×10^{-6}	4.20×10^{-6}
48	4.61×10^{-6}	2.27×10^{-6}	5.13×10^{-6}	3.97×10^{-6}
69	4.48×10^{-6}	1.53×10^{-6}	5.11×10^{-6}	2.46×10^{-6}
97	4.42×10^{-6}	6.43×10^{-7}	4.90×10^{-6}	3.44×10^{-6}
125	3.99×10^{-6}	1.28×10^{-7}	4.57×10^{-6}	2.74×10^{-6}
167	4.12×10^{-6}	3.52×10^{-8}	4.68×10^{-6}	2.25×10^{-6}
277	3.91×10^{-6}	6.36×10^{-9}	4.44×10^{-6}	6.30×10^{-9}
343	3.66×10^{-6}	3.97×10^{-9}	3.89×10^{-6}	5.73×10^{-9}
407	3.60×10^{-6}	6.40×10^{-9}	4.09×10^{-6}	4.09×10^{-9}
517	3.58×10^{-6}	5.32×10^{-9}	4.34×10^{-6}	6.75×10^{-9}
566	1.41×10^{-6}	6.14×10^{-9}	4.60×10^{-6}	4.81×10^{-9}
650	3.48×10^{-6}	3.76×10^{-9}	3.91×10^{-6}	5.98×10^{-9}
683	3.16×10^{-6}	3.85×10^{-9}	3.57×10^{-6}	3.72×10^{-9}

Table A11. Sr concentration of experiments with Sr in the aqueous solution at 23 °C.

	Sr Concentration (mol/kg)			
Day	**SL 5 g/kg RT Sr 0.05_1**	**SL 5 g/kg RT Sr 0.005_1**	**SL 5 g/kg RT Sr 0.05_2**	**SL 5 g/kg RT Sr 0.005_2**
1	4.65×10^{-2}	4.86×10^{-3}	4.65×10^{-2}	5.10×10^{-3}
4	5.08×10^{-2}	4.96×10^{-3}	4.67×10^{-2}	5.22×10^{-3}
6	4.55×10^{-2}	4.89×10^{-3}	4.55×10^{-2}	5.06×10^{-3}
13	4.76×10^{-2}	5.07×10^{-3}	4.73×10^{-2}	5.13×10^{-3}
20	4.71×10^{-2}	4.92×10^{-3}	4.78×10^{-2}	5.07×10^{-3}
34	4.62×10^{-2}	4.79×10^{-3}	4.77×10^{-2}	4.94×10^{-3}
48	4.69×10^{-2}	4.53×10^{-3}	4.41×10^{-2}	4.34×10^{-3}
69	4.54×10^{-2}	4.31×10^{-3}	4.39×10^{-2}	4.41×10^{-3}
97	4.76×10^{-2}	4.35×10^{-3}	4.38×10^{-2}	4.37×10^{-3}
125	5.51×10^{-2}	5.72×10^{-3}	5.43×10^{-2}	5.67×10^{-3}
167	5.40×10^{-2}	6.83×10^{-3}	6.52×10^{-2}	6.07×10^{-3}
277	5.58×10^{-2}	5.64×10^{-3}	5.48×10^{-2}	5.66×10^{-3}
343	5.48×10^{-2}	5.70×10^{-3}	5.45×10^{-2}	5.70×10^{-3}
407	5.51×10^{-2}	5.70×10^{-3}	5.51×10^{-2}	5.67×10^{-3}
517	4.68×10^{-2}	4.50×10^{-3}	4.62×10^{-2}	4.68×10^{-3}
566	4.66×10^{-2}	4.60×10^{-3}	4.70×10^{-2}	4.57×10^{-3}
650	4.70×10^{-2}	4.65×10^{-3}	4.67×10^{-2}	4.64×10^{-3}

Table A12. Sr concentration of Reference experiments with Sr in the aqueous solution at 23 °C.

Sr Concentration Reference without Ra(mol/kg)		
Day	**Reference SL 5 g/kg RT Sr 0.05**	**Reference SL 5 g/kg RT Sr 0.005**
1	4.83×10^{-2}	4.92×10^{-3}
4	4.74×10^{-2}	4.95×10^{-3}
6	4.62×10^{-2}	4.87×10^{-3}
13	4.80×10^{-2}	5.02×10^{-3}
20	4.80×10^{-2}	5.00×10^{-3}
34	4.79×10^{-2}	5.01×10^{-3}
48	4.08×10^{-2}	4.00×10^{-3}
69	4.07×10^{-2}	3.96×10^{-3}
97	4.00×10^{-2}	3.95×10^{-3}
125	5.34×10^{-2}	5.64×10^{-3}
167	1.37×10^{-2}	5.60×10^{-3}
277	5.32×10^{-2}	5.57×10^{-3}
343	5.36×10^{-2}	5.58×10^{-3}
407	5.35×10^{-2}	5.70×10^{-3}
517	4.49×10^{-2}	
566	4.73×10^{-2}	4.57×10^{-3}
650		4.68×10^{-3}

Table A13. Ba concentration of experiments with Sr in the aqueous solution at 23 °C.

Ba Concentration (mol/kg)				
Day	**SL 5 g/kg RT Sr 0.05_1**	**SL 5 g/kg RT Sr 0.005_1**	**SL 5 g/kg RT Sr 0.05_2**	**SL 5 g/kg RT Sr 0.005_2**
1	4.74×10^{-5}	4.68×10^{-5}	5.19×10^{-5}	4.36×10^{-5}
4	5.30×10^{-5}	4.90×10^{-5}	5.39×10^{-5}	4.54×10^{-5}
6	4.96×10^{-5}	4.95×10^{-5}	5.41×10^{-5}	4.63×10^{-5}
13	5.10×10^{-5}	5.06×10^{-5}	5.63×10^{-5}	4.56×10^{-5}
20	5.23×10^{-5}	5.13×10^{-5}	5.69×10^{-5}	4.76×10^{-5}
34	5.19×10^{-5}	5.41×10^{-5}	5.74×10^{-5}	4.69×10^{-5}
48	5.92×10^{-5}	6.13×10^{-5}	6.31×10^{-5}	5.06×10^{-5}
69	5.95×10^{-5}	6.13×10^{-5}	6.42×10^{-5}	5.31×10^{-5}
97	5.89×10^{-5}	6.30×10^{-5}	6.05×10^{-5}	5.17×10^{-5}
125	5.04×10^{-5}	4.82×10^{-5}	5.49×10^{-5}	4.06×10^{-5}
167	5.01×10^{-5}	6.00×10^{-5}	6.78×10^{-5}	4.50×10^{-5}
277	4.92×10^{-5}	5.19×10^{-5}	5.16×10^{-5}	4.68×10^{-5}
343	5.11×10^{-5}	5.27×10^{-5}	5.01×10^{-5}	5.15×10^{-5}
407	4.88×10^{-5}	5.61×10^{-5}	5.26×10^{-5}	5.21×10^{-5}
517	4.55×10^{-5}	5.78×10^{-5}	5.11×10^{-5}	5.93×10^{-5}
566	4.93×10^{-5}	6.09×10^{-5}	5.13×10^{-5}	5.92×10^{-5}
650	4.65×10^{-5}	6.19×10^{-5}	4.86×10^{-5}	6.30×10^{-5}

Table A14. Sr concentration of Reference experiments with Sr in the aqueous solution at 23 °C.

Sr Concentration Reference without Ra (mol/kg)		
Day	**Reference SL 5 g/kg RT Sr 0.05**	**Reference SL 5 g/kg RT Sr 0.005**
1	3.77×10^{-5}	4.51×10^{-5}
4	3.70×10^{-5}	4.85×10^{-5}
6	3.79×10^{-5}	4.88×10^{-5}
13	3.71×10^{-5}	4.75×10^{-5}
20	3.75×10^{-5}	4.76×10^{-5}
34	3.83×10^{-5}	4.86×10^{-5}
48	4.03×10^{-5}	5.16×10^{-5}
69	4.19×10^{-5}	5.23×10^{-5}
97	4.03×10^{-5}	5.12×10^{-5}
125	3.27×10^{-5}	4.55×10^{-5}
167	3.21×10^{-5}	
277	3.16×10^{-5}	4.53×10^{-5}
343	3.34×10^{-5}	4.34×10^{-5}
407	3.31×10^{-5}	4.48×10^{-5}
517	3.52×10^{-5}	4.51×10^{-5}
566	3.49×10^{-5}	4.28×10^{-5}
650	3.52×10^{-5}	4.01×10^{-5}

References

1. Putnis, A.; Putnis, C.V. The mechanism of reequilibration of solids in the presence of a fluid phase. *J. Solid State Chem.* **2007**, *180*, 1783–1786. [CrossRef]
2. Hellmann, R.; Wirth, R.; Daval, D.; Barnes, J.-P.; Penisson, J.-M.; Tisserand, D.; Epicier, T.; Florin, B.; Hervig, R.L. Unifying natural and laboratory chemical weathering with interfacial dissolution–reprecipitation: A study based on the nanometer-scale chemistry of fluid–silicate interfaces. *Chem. Geol.* **2012**, *294–295*, 203–216. [CrossRef]
3. Konrad-Schmolke, M.; Halama, R.; Wirth, R.; Thomen, A.; Klitscher, N.; Morales, L.; Schreiber, A.; Wilke, F.D.H. Mineral dissolution and reprecipitation mediated by an amorphous phase. *Nat. Commun.* **2018**, *9*, 1637. [CrossRef] [PubMed]
4. Lindner, M.; Saldi, G.D.; Carrocci, S.; Bénézeth, P.; Schott, J.; Jordan, G. On the growth of anhydrous Mg-bearing carbonates—Implications from norsethite growth kinetics. *Geochim. Cosmochim. Acta* **2018**, *238*, 424–437. [CrossRef]
5. Heberling, F.; Vinograd, V.L.; Polly, R.; Gale, J.D.; Heck, S.; Rothe, J.; Bosbach, D.; Geckeis, H.; Winkler, B. A thermodynamic adsorption/entrapment model for selenium(IV) coprecipitation with calcite. *Geochim. Cosmochim. Acta* **2014**, *134*, 16–38. [CrossRef]
6. Heberling, F.; Metz, V.; Böttle, M.; Curti, E.; Geckeis, H. Barite recrystallization in the presence of 226 Ra and 133 Ba. *Geochim. Cosmochim. Acta* **2018**. [CrossRef]
7. Brandt, F.; Curti, E.; Klinkenberg, M.; Rozov, K.; Bosbach, D. Replacement of barite by a (Ba, Ra) SO_4 solid solution at close-to-equilibrium conditions: A combined experimental and theoretical study. *Geochim. Cosmochim. Acta* **2015**, *155*, 1–15. [CrossRef]
8. Prieto, M.; Heberling, F.; Rodríguez-Galán, R.M.; Brandt, F. Crystallization behavior of solid solutions from aqueous solutions: An environmental perspective. *Prog. Cryst. Growth Charact. Mater.* **2016**, *62*, 29–68. [CrossRef]
9. Rodríguez-Galán, R.M.; Prieto, M. Interaction of Nonideal, Multicomponent Solid Solutions with Water: A Simple Algorithm to Estimate Final Equilibrium States. *Geochem. Geophys. Geosyst.* **2018**, *19*, 1348–1359. [CrossRef]
10. Klinkenberg, M.; Brandt, F.; Breuer, U.; Bosbach, D. Uptake of Ra during the recrystallization of barite: A microscopic and time of flight-secondary ion mass spectrometry study. *Environ. Sci. Technol.* **2014**, *48*, 6620–6627. [CrossRef] [PubMed]

11. Weber, J.; Barthel, J.; Brandt, F.; Klinkenberg, M.; Breuer, U.; Kruth, M.; Bosbach, D. Nano-structural features of barite crystals observed by electron microscopy and atom probe tomography. *Chem. Geol.* **2016**, *424*, 51–59. [CrossRef]
12. Weber, J.; Barthel, J.; Klinkenberg, M.; Bosbach, D.; Kruth, M.; Brandt, F. Retention of226Ra by barite: The role of internal porosity. *Chem. Geol.* **2017**, *466*, 722–732. [CrossRef]
13. Rosenberg, Y.O.; Metz, V.; Oren, Y.; Volkman, Y.; Ganor, J. Co-precipitation of radium in high ionic strength systems: 2. Kinetic and ionic strength effects. *Geochim. Cosmochim. Acta* **2011**, *75*, 5403–5422. [CrossRef]
14. Zhang, T.; Gregory, K.; Hammack, R.W.; Vidic, R.D. Co-precipitation of Radium with Barium and Strontium Sulfate and Its Impact on the Fate of Radium during Treatment of Produced Water from Unconventional Gas Extraction. *Environ. Sci. Technol.* **2014**, *48*, 4596–4603. [CrossRef] [PubMed]
15. International Atomic Energy Agency (IAEA). *The Environmental Behaviour of Radium: Revised Edition*; International Atomic Energy Agency: Vienna, Austria, 2014.
16. Garner, J.; Cairns, J.; Read, D. NORM in the East Midlands' oil and gas producing region of the UK. *J. Environ. Radioact.* **2015**, *150*, 49–56. [CrossRef] [PubMed]
17. Berner, U. *Solubility of Radionuclides in a Bentonite Environment for Provisional Safety Analyses for SGT-E2*; Paul Scherrer Institut, Villigen PSI: Wettingen, Switzerland, 2014.
18. SKB. *Long-Term Safety for the Final Repository of Spent Nuclear Fuel at Forsmark Main Report of the Sr-Site Project I–III*; SKB: Stockholm, Sweden, 2011.
19. Vinograd, V.L.; Brandt, F.; Rozov, K.; Klinkenberg, M.; Refson, K.; Winkler, B.; Bosbach, D. Solid-aqueous equilibrium in the $BaSO_4$-$RaSO_4$-H_2O system: First-principles calculations and a thermodynamic assessment. *Geochim. Cosmochim. Acta* **2013**, *122*, 398–417. [CrossRef]
20. Vinograd, V.L.; Kulik, D.A.; Brandt, F.; Klinkenberg, M.; Weber, J.; Winkler, B.; Bosbach, D. Thermodynamics of the solid solution—Aqueous solution system (Ba, Sr, Ra) SO_4 + H_2O: I. The effect of strontium content on radium uptake by barite. *Appl. Geochem.* **2018**, *89*, 59–74. [CrossRef]
21. Vinograd, V.L.; Kulik, D.A.; Brandt, F.; Klinkenberg, M.; Weber, J.; Winkler, B.; Bosbach, D. Thermodynamics of the solid solution—Aqueous solution system (Ba, Sr, Ra) SO_4 + H_2O: II. Radium retention in barite-type minerals at elevated temperatures. *Appl. Geochem.* **2018**, *93*, 190–208. [CrossRef]
22. Klinkenberg, M.; Weber, J.; Barthel, J.; Vinograd, V.; Poonoosamy, J.; Kruth, M.; Bosbach, D.; Brandt, F. The solid solution–aqueous solution system (Sr, Ba, Ra) SO_4 + H_2O: A combined experimental and theoretical study of phase equilibria at Sr-rich compositions. *Chem. Geol.* **2018**, *497*, 1–17. [CrossRef]
23. Jucker, H.; Treadwell, W.D. Über die Mitfällung von Radium mit Bariumsulfat. *Helv. Chim. Acta* **1954**, *37*, 2002–2010. [CrossRef]
24. Ceccarello, S.; Black, S.; Read, D.; Hodson, M.E. Industrial radioactive barite scale: Suppression of radium uptake by introduction of competing ions. *Miner. Eng.* **2004**, *17*, 323–330. [CrossRef]
25. Ling, F.T.; Hunter, H.A.; Fitts, J.P.; Peters, C.A.; Acerbo, A.S.; Huang, X.; Yan, H.; Nazaretski, E.; Chu, Y.S. Nanospectroscopy Captures Nanoscale Compositional Zonation in Barite Solid Solutions. *Sci. Rep.* **2018**, *8*, 13041. [CrossRef] [PubMed]
26. Jindra, S.A.; Bertagni, A.L.; Bracco, J.N.; Higgins, S.R. Hydrothermal Atomic Force Microscopy Investigation of Barite Growth: Role of Spectator Ions in Elementary Step Edge Growth Kinetics and Hillock Morphology. *Cryst. Growth Des.* **2017**, *17*, 6085–6095. [CrossRef]
27. Kowacz, M.; Putnis, A. The effect of specific background electrolytes on water structure and solute hydration: Consequences for crystal dissolution and growth. *Geochim. Cosmochim. Acta* **2008**, *72*, 4476–4487. [CrossRef]
28. Risthaus, P.; Bosbach, D.; Becker, U.; Putnis, A. Barite scale formation and dissolution at high ionic strength studied with atomic force microscopy. *Colloids Surf. A Physicochem. Eng. Asp.* **2001**, *191*, 201–214. [CrossRef]
29. Ruiz-Agudo, E.; Putnis, C.V.; Wang, L.; Putnis, A. Specific effects of background electrolytes on the kinetics of step propagation during calcite growth. *Geochim. Cosmochim. Acta* **2011**, *75*, 3803–3814. [CrossRef]
30. Godinho, J.R.A.; Stack, A.G. Growth Kinetics and Morphology of Barite Crystals Derived from Face-Specific Growth Rates. *Cryst. Growth Des.* **2015**, *15*, 2064–2071. [CrossRef]
31. Curti, E.; Fujiwara, K.; Iijima, K.; Tits, J.; Cuesta, C.; Kitamura, A.; Glaus, M.A.; Müller, W. Radium uptake during barite recrystallization at 23 $\pm$ 2 °C as a function of solution composition: An experimental 133Ba and 226Ra tracer study. *Geochim. Cosmochim. Acta* **2010**, *74*, 3553–3570. [CrossRef]

32. Kulik, D.A.; Wagner, T.; Dmytrieva, S.V.; Kosakowski, G.; Hingerl, F.F.; Chudnenko, K.V.; Berner, U.R. GEM-Selektor geochemical modeling package: Revised algorithm and GEMS3K numerical kernel for coupled simulation codes. *Comput. Geosci.* **2013**, *17*, 1–24. [CrossRef]
33. Wagner, T.; Kulik, D.A.; Hingerl, F.F.; Dmytrieva, S.V. GEM-Selektor geochemical modeling package: TSolMod library and data interface for multicomponent phase models. *Can. Mineral.* **2012**, *50*, 701–723. [CrossRef]
34. Helgeson, H.C.; Kirkham, D.H.; Flowers, G.C. Theoretical prediction of the thermodynamic behavior of aqueous electrolytes by high pressures and temperatures; IV, Calculation of activity coefficients, osmotic coefficients, and apparent molal and standard and relative partial molal properties to 600 degrees C and 5 kb. *Am. J. Sci.* **1981**, *281*, 1249–1516. [CrossRef]
35. Johnson, J.W.; Oelkers, E.H.; Helgeson, H.C. SUPCRT92: A software package for calculating the standard molal thermodynamic properties of minerals, gases, aqueous species, and reactions from 1 to 5000 bar and 0 to 1000 °C. *Comput. Geosci.* **1992**, *18*, 899–947. [CrossRef]
36. Thoenen, T.; Hummel, W.; Berner, U.; Curti, E. *The PSI/Nagra Chemical Thermodynamic Database 12/07*; Nuclear Energy and Safety Research Department Laboratory for Waste Management (LES): New York, NY, USA, 2014.
37. Blount, C.W. Barite solubilities thermodynamic and quantities up to 300 °C and 1400 bars. *Am. Mineral.* **1977**, *62*, 942–957.
38. Monnin, C.; Galinier, C. The solubility of celestite and barite in electrolyte solutions and natural waters at 25 °C: A thermodynamic study. *Chem. Geol.* **1988**, *71*, 283–296. [CrossRef]
39. Tokunaga, K.; Kozai, N.; Takahashi, Y. A new technique for removing strontium from seawater by coprecipitation with barite. *J. Hazard. Mater.* **2018**, *359*, 307–315. [CrossRef] [PubMed]
40. YuHang, C.; Asenjo, A.; Sánchez-Pastor, N.; Fernández-Díaz, L.; Gómez, J.; Pina, C.M. Growth of $Ba_xSr_{1-x}SO_4$ nano-steps on barite (001) face. *Surf. Sci.* **2007**, *601*, 381–389. [CrossRef]
41. Weber, J.; Bracco, J.N.; Poplawsky, J.D.; Ievlev, A.V.; More, K.L.; Lorenz, M.; Bertagni, A.L.; Jindra, S.A.; Starchenko, V.; Higgins, S.R.; et al. Unraveling the Effects of Strontium Incorporation on Barite Growth—In Situ and Ex Situ Observations Using Multiscale Chemical Imaging. *Cryst. Growth Des.* **2018**, *18*, 5521–5533. [CrossRef]
42. Sánchez-Pastor, N.; Pina, C.M.; Astilleros, J.M.; Fernández-Díaz, L.; Putnis, A. Epitaxial growth of celestite on barite (001) face at a molecular scale. *Surf. Sci.* **2005**, *581*, 225–235. [CrossRef]
43. Grambow, B.; Vandenborre, J.; Suzuki-Muresan, T.; Philippini, V.; Abdelouas, A.; Deniard, P.; Jobic, S. Solubility equilibrium and surface reactivity at solid/liquid interfaces of relevance to disposal of nuclear waste. *J. Chem. Thermodyn.* **2017**, *114*, 172–181. [CrossRef]
44. Bracco, J.; Lee, S.S.; Stubbs, J.; Eng, P.; Weber, J.; Fenter, P.; Kubicki, J. Strontium adsorption at the barite (001)—Water interface. In *Abstracts of Papers of the American Chemical Society*; American Chemical Society: Washington, DC, USA, 2018.